USING CHODIN TO SIMULATE COHERENT LIGHT SCATTERING DYNAMICS ON BIOLOGICAL SUSPENSIONS[#]

D. CHICEA*, R. CHICEA**, LIANA MARIA CHICEA**

*Physics Department, "Lucian Blaga" University of Sibiu, 7–9, Dr. Ion Rațiu St., Sibiu, 550012, Romania, dan.chicea@ulbsibiu.ro
**"Victor Papilian" Faculty of Medicine, "Lucian Blaga" University of Sibiu

Abstract. When coherent light passes through a transparent fluid having scattering centers (SC) in suspension the result of the far field interference is a "speckled" image. In suspension the SCs have a complex sedimentation and Brownian motion. Consequently, the biospeckle image is not static but presents time fluctuations. A computer code to simulate the dynamics of the coherent light scattering on biological suspensions was written and used to investigate typical biological suspensions like erythrocytes. The calculated far field intensity variation was analyzed using the Dynamic Light Scattering particle sizing technique and the simulation results were found to be realistic. Practical applications are suggested based on the simulation results.

Key words: suspensions, computer simulation, biospeckles, image processing.

INTRODUCTION

If a medium having scattering centers is illuminated with coherent light, a non-uniformly illuminated image is obtained, currently named speckled image, having a statistical distribution of the intensity over the interference field. The speckled image appears as a result of the interference of the wavelets scattered by the scattering centers, each wavelet having a different phase and amplitude in each location of the interference field. The image changes in time as a consequence of the scattering centers complex movement of sedimentation and Brownian motion. This produces fluctuations of the image intensity in each location of the interference field. These fluctuations give the aspect of "boiling speckles" [5, 8].

The speckled image can be observed either in free space and is called objective speckle or on the image plane of a diffuse object illuminated by a

---

[#]This study was presented in the *National Conference of Biophysics*, Cluj-Napoca, October, 2009.

coherent source; it is named subjective speckle in [8]. The review paper [5] calls the two types of speckled images far field speckle and image speckle. In this work the objective speckle, respectively the far field speckle is considered.

The speckle parameters like size, contrast, intensity and polarization carry information on the scattering media. Dynamical speckle analysis has become a current method to characterize the dynamic behavior of the scattering medium such as flow, sedimentation and Brownian motion. The motion of the speckle field was analyzed by correlometric methods [1, 3, 7] or by laser speckle contrast analysis [4, 20]. In this work the far field interference was considered. A computer code to simulate the dynamics of the interference pattern, to calculate and write the digital movie of the interference field or a time series was developed and tested. Details are presented in the next section.

THE ALGORITHM

The program considers a coherent light having the wavelength of 632 nm to be incident on a cuvette containing the suspension. The active area of the glass cuvette was $1 \times 1 \times 12$ mm, typical for a thick cuvette. The far field interference pattern was calculated at a distance D apart from the simulated cuvette. The schematic of the computer simulation setup is presented in Fig. 1.

The input parameters for the simulation are: the total number of SCs, the wavelength, an arbitrary intensity of the electric field E_0, the cuvette active area coordinates, the cuvette-screen distance D, the x and y coordinates of the corner of the calculation area, the "pixel" dimension on the screen, the number of pixels on X and Y directions, the total number of time steps (frames) to be calculated, the number of time steps per second (frames per second), the area (cross section) and the volume of an individual SC, the light scattering anisotropy parameter g, the dynamic viscosity coefficient of the fluid and finally the temperature, which is required for the Brownian motion simulation.

First the scattering centers positions were generated in the active area of the cuvette using random numbers with uniform distribution. The complex amplitude of the electric field scattered by each scattering center was added for each pixel the assumed conversion matrix area was divided into. The pixel size on the simulated interference field was chosen to be the same as the pixel size of the CCD matrix of a web camera that had the optical system removed. The CCD was used to record the far field interference movie of the real system that was later on simulated, in order to compare the real movie with the calculated movie.

The single act light scattering anisotropy on a SC was modeled using the one parameter, single scattering Henyey Greenstein phase function [11, 13] (Eq. 1).

$$f(\mu) = \frac{1}{2} \frac{1 - g^2}{(1 - 2\mu g + g^2)^{\frac{3}{2}}} \tag{1}$$

where $\mu = \cos(\theta)$. The anisotropy parameter, g, is currently defined as the mean cosine of the polar scattering angle θ, $g = \langle \cos(\theta) \rangle$. Consequently, for light scattering strongly peaked in the forward direction, the anisotropy parameter g is close to 1 while for isotropic scattering it is zero.
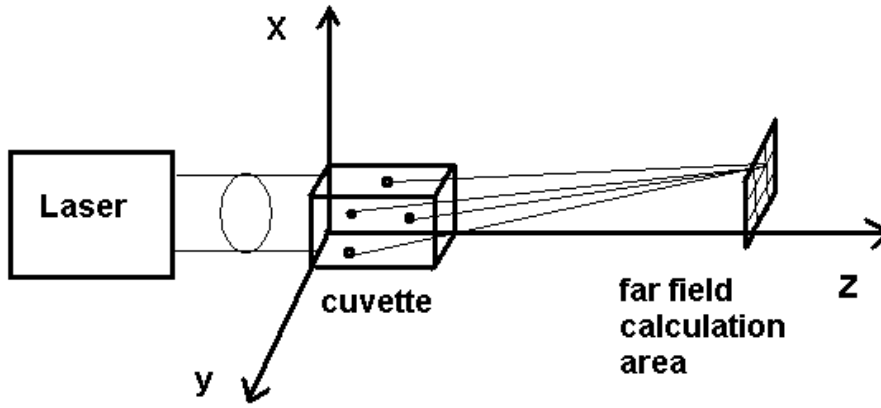

Fig. 1. The schematic of the computer simulation.

The electric field amplitude of the light scattered by an individual SC, which is added (using complex numbers) to the electric field intensity of the interference field of a specific pixel on the screen, is proportional to the integral of the f function in Eq. (1) over the cosines of the polar angle interval covered by the pixel, $[\mu_1, \mu_2]$ and with $\Delta\varphi$, the azimuthal angle interval and is described by equation (2):

$$E(d, \theta, \phi) = \frac{E_0 S_0}{d} \frac{1 - g^2}{2g} \left[\left(\frac{1}{\sqrt{1 + g^2 - 2\mu_2 g}} \right) - \left(\frac{1}{\sqrt{1 + g^2 - 2\mu_1 g}} \right) \right] \Delta\phi \tag{2}$$

In Eq. (2) d is the individual SC-pixel distance, E_0 an arbitrary constant, S_0 the SC area (cross section).

At each simulation time step the SCs were moved in the active area considering both the uniform sedimentation and the Brownian motion and the details are presented further on.

MODELING SEDIMENTATION

The sedimentation of the SC carries on with a constant velocity, which is the consequence of the null resultant of three forces: gravity, buoyant force and the viscous force in laminar flow regime (Stokes). Considering the SC with a spherical shape, the velocity is given by equation (3):

$$v_s = \frac{2r^2 g}{9\eta}(\rho - \rho_0) \tag{3}$$

where r is the radius of the sphere, ρ is the density of the scattering center, ρ_0 is the fluid density, η is the dynamic viscosity coefficient of the fluid. The sedimentation was modeled for each SC individually by changing the position with a distance equal to the v_s times the time step. The time step for modeling the sedimentation is the inverse of the framerate, which is one of the input parameters. The framerate is actually the framerate used in calculating a movie or the sampling rate, which is the time interval between two consecutive readings of the data acquisition system used in recording a time series during a laboratory experiment.

BROWNIAN MOTION MODELING

The Brownian motion velocity can be estimated using the thermal equilibrium velocity [1] (Eq. 4):

$$v_t = \frac{3k_B T}{m} \tag{4}$$

In Eq. (4) k_B is Boltzman's constant, T is the absolute temperature and m is the mass of the particle in thermal equilibrium with the environment.

For a red blood cell (RBC), having a typical radius of 4 μm [10, 11] in isotonic saline aqueous suspension the sedimentation velocity at room temperature, calculated with (3) is around 3.5×10^{-6} m/s and the Brownian motion velocity, calculated with (4) is around 3.5×10^{-4} m/s. Milk particles in suspension were first used as SC in this computer simulation. Papers like [15] point out that the milk fat particles have a size distribution that depends on the machining that was used for skimming the milk. For unskimmed milk a typical particle size (diameter) that can be used is 1 μm. Latex balls are another preferred SC when doing calibration for light scattering, speckle size and contrast analysis [16, 17]. Typical values of the sedimentation and Brownian motion velocity for RBC, milk particles and latex balls with several values of the diameter are presented in Table 1.

Examining Table 1 we notice that the Brownian motion velocity is much bigger than the sedimentation velocity. Moreover, the Brownian motion direction has a random orientation.

Table 1

The thermal and the sedimentation velocities for typical SCs

Particle (SC)tt	Diameter (μm)	Brownian velocity (m/s)	Sedimentation velocity (m/s)
RBC	8	3.5×10^{-4}	3.5×10^{-6}
Latex ball	4	5.5×10^{-4}	1.7×10^{-6}
Latex ball	2	1.6×10^{-3}	4.3×10^{-7}
Latex ball	1	4.4×10^{-3}	1.1×10^{-7}
Milk fat particle	1	5×10^{-3}	2.7×10^{-8}
Latex ball	0.5	1.2×10^{-2}	2.7×10^{-8}

The Brownian motion was modeled differently, though individually for each SC. The Maxwell-Boltzman velocity distribution is actually the product of the three velocity distribution functions for one dimension:

$$f_v(v_i) = \sqrt{\frac{m}{2\pi k_B T}} \exp\left(-\frac{m v_i^2}{2 k_B T}\right) \tag{5}$$

In Eq. (5) m is the mass of the particle in thermal equilibrium with the environment and i can be either x, y or z. At each simulation time step the velocity values for v_x, v_y and v_z of each SC were therefore generated using random numbers with a normal distribution having the variance $\frac{k_B T}{m}$.

It should be noted that in order to have a realistic Brownian motion modeling, the time step for the Brownian motion must be different from the time step used to model the sedimentation and details on assessing it are presented below.

If particles are diffusing in a solvent, the number density $n(\vec{r}, t)$ variation in time is described by the basic equation:

$$\frac{\partial n}{\partial t} - D\nabla^2 n = 0 \tag{6}$$

also called the diffusion equation, where D is the diffusion coefficient. Since the probability $P(\vec{r}, t)$ of finding a particle in a small volume is directly proportional to the number density, this leads to equation (7):

$$\frac{\partial P}{\partial t} - D\nabla^2 P = 0 \tag{7}$$

The diffusion coefficient D can be related to other properties of the system like the temperature T and μ, the mobility, which is the ratio of drift velocity to driving force when the particle is pushed through the fluid by an external force, by invoking the Einstein relation:

$$D = k_{\mathrm{B}}T\mu \qquad (8)$$

The mobility can be calculated from classical hydrodynamics for spheres of radius R which are large compared to the surrounding molecules, driven by an external force F_{ext}, in laminar flow regime (Stokes):

$$\vec{F}_{\text{ext}} = 6\pi\eta R\vec{v}_{\text{drift}}, \quad \vec{v}_{\text{drift}} = \mu \cdot \vec{F} \quad \Rightarrow \quad \mu = \frac{1}{6\pi\eta R} \qquad (9)$$

Substituting μ in Eq. (8) we find the diffusion coefficient for spheres of radius R to be:

$$D = \frac{k_{\mathrm{B}}T}{6\pi\eta R} \qquad (10)$$

We want a solution to this equation with the initial condition that the particle is at $r = 0$ and $t = 0$:

$$P(0,0) = \delta(\vec{r}) \qquad (11)$$

Such a solution, that can be proven by direct differentiation, is:

$$P(\vec{r}, t) = (4\pi D\, t)^{-\frac{3}{2}} \exp\left(-\frac{r^2}{4D\, t}\right) \qquad (12)$$

The result from the diffusion equation, the probability distribution $P(\vec{r}, t)$, must be connected with a real measurable quantity. The second moment of the P distribution $\langle r^2 \rangle$ draws a useful relationship about diffusion and, taking advantage of the radial symmetry and using polar coordinates, we find:

$$\langle r^2(t) \rangle = \int\limits_0^\infty \int\limits_0^\pi \int\limits_0^{2\pi} r^2 P(\vec{r}, t) r^2 \sin\theta d\theta d\varphi = 6Dt \qquad (13)$$

First a set of simple computer diffusion experiments was done. 5000 particles were used in order to have a good statistics and their positions were $(0,0,0)$ in Cartesian coordinates at time $t = 0$. A certain value was selected for the Brownian motion time step modeling and the system was let to evolve for a total preselected time t. At each time step the particles velocities were generated having a Maxwell-Boltzman velocity distribution, described by Eq. (5), and the new positions were calculated for each particle adding to the old positions the velocity times the time step. When the preset time elapsed, the positions were saved, $\langle r^2 \rangle$ was computed and finally D_{comp} was calculated from Eq. (13) for that particular value of the time

step. Different time step values were used for each experiment, a curve was drawn with D_{comp} values *versus* the time step. The time step value that produced a D_{comp} value equal to the one calculated with Eq. (10) was chosen for the light scattering dynamics simulation.

For 3.77 μm radius particles (about the size of a RBC) in water at 293.15 K the diffusion coefficient calculated with Eq. (11) is 5.67×10^{-14} m^2s^{-1} and the Brownian motion time step that produces a D_{comp} that matches this value is 5.046 $\times 10^{-6}$ s. Fig. 2 presents the variation of the computed diffusion coefficient with the Brownian motion time step. We notice that for the small time step range that was used for assessing the Brownian motion time step the variation appears to be linear.

At each time step of the simulation all the SCs are relocated. The calculation procedure was repeated, the image area intensity was recalculated, an AVI type file was produced and the simulated photodetector signal in a specific location was recorded. The procedure is repeated till the desired number of frames is reached.

VALIDATION OF THE RESULTS

A time series was calculated for different simulated suspensions, having several values of the diameter, from 30 nm to 30 μm. For 3.77 μm particles (about the size of a RBC) in water at 293.15 K, a calculated time series is presented in Fig. 3.
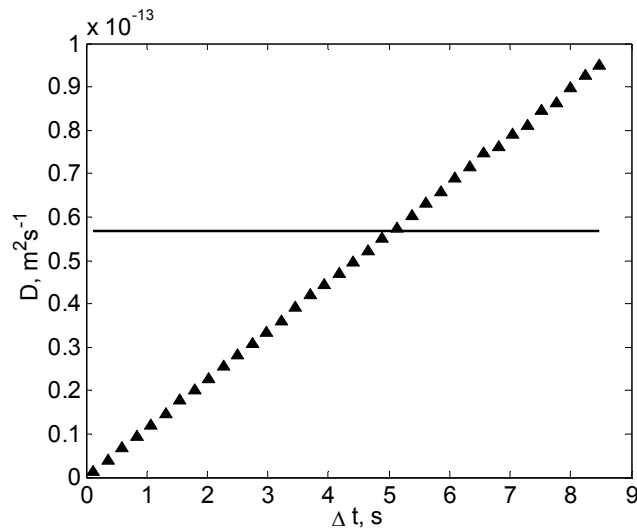

Fig. 2. The computed values of the diffusion coefficient (triangles) *versus* the preset time step and the Einstein diffusion coefficient (solid line) for 3.77 μm particles in suspension.

A good procedure to validate the results would be to analyze the time series using the Dynamic Light Scattering technique (DLS).

As proved in [8, 11, 18] the width of the autocorrelation function of the time series is proportional to the diffusion coefficient, which, on its turn, depends on the particle diameter. This leads to a fast procedure for measuring the particle diameter. An improved version is described further on in this section. The early experimental works [6, 14] and the further theoretical treatises [2, 9, 12] proved the assumption that the power spectrum of the intensity of the light scattered by particles in suspension can be linked to the probability density function (PDF). This link between the PDF and the power spectrum is a consequence of the translation of the relative motion of the scattering particles into phase differences of the scattered light. Thus, spatial correlations are translated into phase correlations, which are manifested in the usage of the Wiener-Khintchine-Theorem, relating the power spectrum to the autocorrelation of a process. The phase correlations lead to fluctuations in the intensity of the scattered light recorded using a detector and a data acquisition system, in a typical experimental setup as presented in Fig. 1.

By subtracting the average intensity from the recorded time series and calculating the square of the intensity we obtain the power time series. The Fourier transform of the power time series is the power spectrum. We can compare the spectrum calculated from the experimental data with the theoretically expected spectrum, namely the functional form of the Lorentzian line $S(f)$ (Eq. 14).
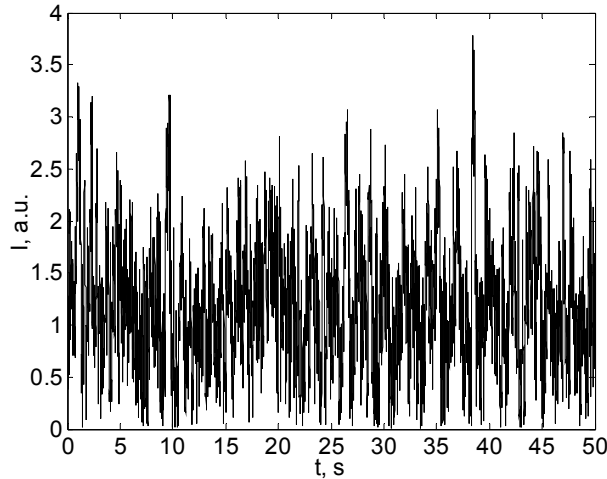

Fig. 3. A computed time series for 3.77 μm particles in water at 293.15 K.

$$S(f) = a_0 \frac{a_1}{(2\pi f) + a_1^2} \tag{14}$$

The Lorentzian line $S(f)$ has two free parameters a_0 and a_1 and is fit to the power spectrum using a non-linear minimization procedure to minimize the distance between the data-set and the line. The possibility to fit the whole function is advantageous compared to the alternative method described in [6, 17, 20], where the $f_{\frac{1}{2}}$ (the frequency where half-maximal-height is reached) was measured, since it takes more data points into account, thus increasing the quality of the fit.

Once the fit is completed and the parameters are found, the diameter of the SCs can be assessed as the double of the radius R. The radius can be derived as a function of the fitted parameter a_1 and other known quantities using Eq. (2):

$$R = \frac{2k_B T K^2}{6\pi\eta a_1} \quad \text{where} \quad K = \frac{4\pi n}{\lambda}\sin\left(\frac{\theta}{2}\right) \qquad (15)$$

In Eq. (15) θ is the scattering angle, n is the refractive index of the scattering particles and λ is the wavelength of the laser radiation. The cuvette-detector distance D was 0.6 m and x was 0.6 m making the scattering angle θ equal to 45°.

The PSD (scattered line) and the fitted Lorentzian line (the smooth line) for the time series presented in Fig. 3 are presented in Fig. 4.
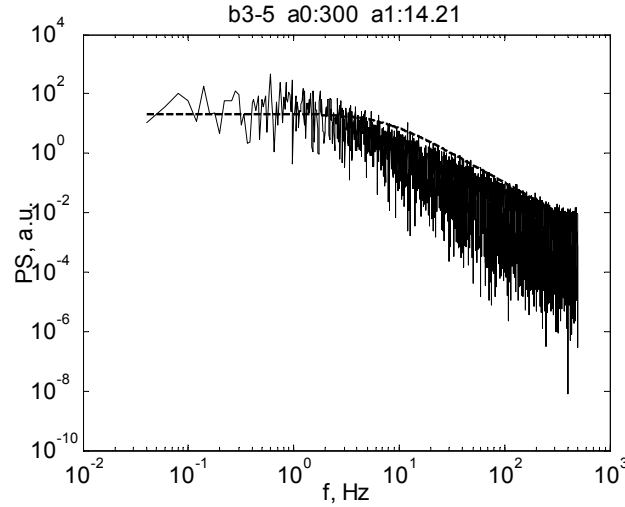

Fig. 4. The PSD (scattered line) and the fitted Lorentzian line (dashed)
for the time series simulated for 3.77 μm particles in water at 293.15 K.

The parameters of the Lorentzian line found from the fit are: a_0 = 300 and a_1 = 14.21. Using Eq. (15) we found that the SCs have an average diameter of 3.91 μm, which is very close to 3.77 μm that was used in computing the time series.

Another way to validate the results is to compare the simulated data with the experimental data. Another time series was computed for diluted milk, which has 1 μm diameter fat particles as scattering centers [15]. The time step used for simulating the Brownian motion, as described above, was 4.0159×10^{-7} s. The pixel size was chosen to be exactly the same as the size of the detector. The experiment in real life with diluted milk having the same dilution and the same experimental setup as in Fig. 1, with the same parameters, was performed as well. The autocorrelation function of each of the time series calculated with the code and from the experiment was calculated with Eq. (16) [5]:

$$A(\tau) = \frac{\langle I(\vec{r},t)I(\vec{r},t+\tau) \rangle}{\langle I(\vec{r},t)I(\vec{r},t) \rangle} \qquad (16)$$

where the angle brackets denote averages over time t, r represents the position of the detector, and τ is the correlation time.

The normalized autocorrelation function decreases from 1 and we can define the autocorrelation time (ACT) as the time when the autocorrelation function decreases to $\frac{1}{e}$. The time step for simulating the Brownian motion, which is different from the time step used to simulate sedimentation, was chosen to produce the same autocorrelation function and ACT as for the experimental time series.
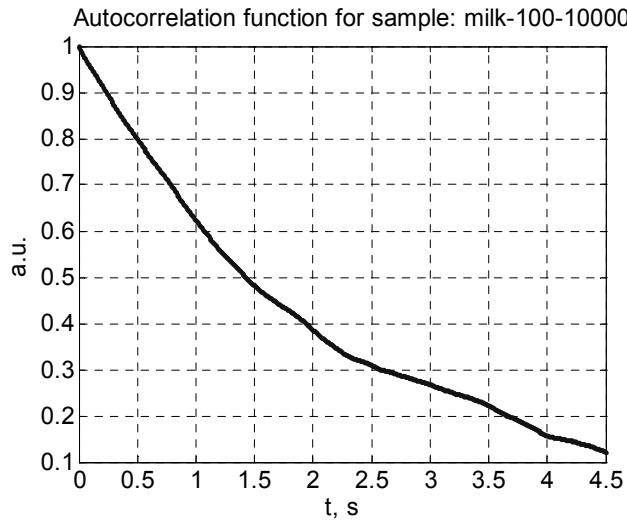

Fig. 5. The autocorrelation function of a calculated time series for a milk suspension, 10^{-6} volume ratio dilution.

Fig. 5 presents the time series calculated for diluted milk, 10^{-6} volume ratio and Fig. 6 the autocorrelation time of the experimentally recorded time series.

Examining Fig. 4 we notice that the PSD of the calculated time series is very close to the Lorentzian line and that the calculated diameter of the SCs is very close of the diameter used in calculating the data. Moreover, examining Figs. 5 and 6 we notice that the aspect of autocorrelation function is the same for the calculated and the experimentally recorded time series and the autocorrelation time is around 2 seconds for both the experimental and the simulated series. These validation procedures confirm that the results of the computer simulation are realistic.
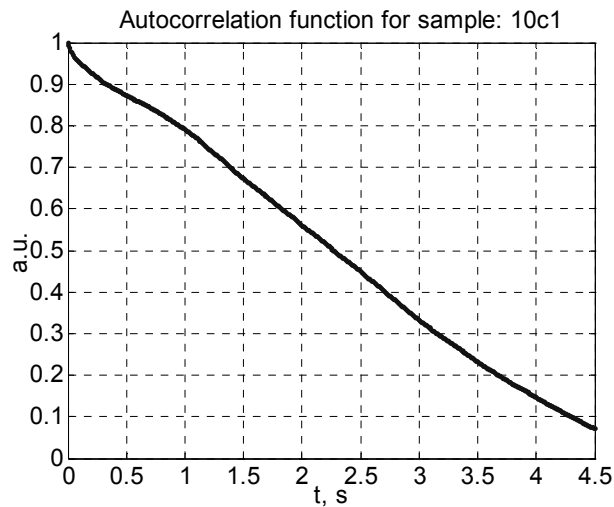

Fig. 6. The autocorrelation function of the experimentally recorded time series, using the same configuration and dilution.

RESULTS

The simulation program was run having as input data parameters of different SCs like fat particles in milk and RBCs. The calculated movie presents the "boiling speckle" aspect and is similar in respect to aspect and dynamics with the movie recorded during a laboratory coherent light scattering experiment on the real suspension. A frame from the calculated movie is presented in Fig. 7.

The input parameters were adjusted to simulate the RBCs in isotonic saline suspension complex movement, composed of both the sedimentation and the Brownian motion. The sedimentation velocity was not calculated using Eq. (3) but was given as input data. Different values from 0 to 70 mm/h were used. The Erythrocyte Sedimentation Rate (ESR) is a standard laboratory test performed on whole human blood, where the velocity of the RBC sedimentation is measured. When it is increased it is an indication of the presence of an inflammatory disease.

The simulation described in this paper deals with different ESR values. The RBCs were modeled as spheres having a 3.77 μm diameter, which is not so close to reality, as the RBC shape is closer to a disk rather than a sphere. The backscattered configuration was chosen this time, as the undiluted blood is opaque to visible light.
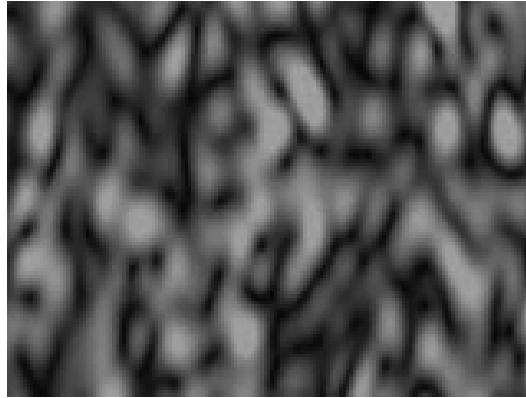

Fig. 7. A calculated frame of the movie for diluted milk, 10^{-6} volume ratio.

The ACT was calculated for each series and the variation of the ACT with the sedimentation velocity is presented in Fig. 8.
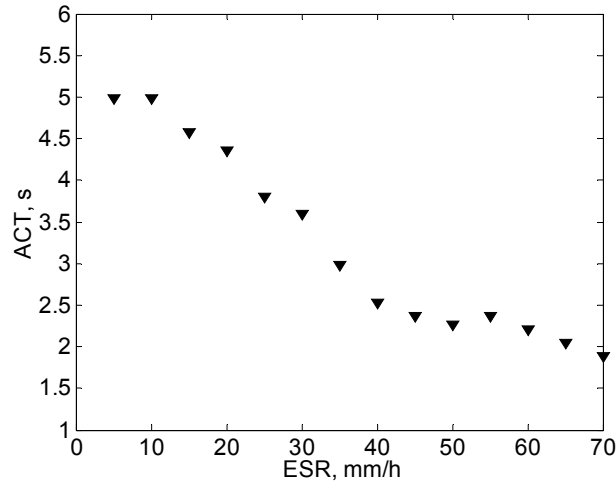

Fig.8. The autocorrelation time *versus* ESR.

These results are consistent with the speckle statistics theory. If a flowing fluid has SCs in suspension, the autocorrelation time has a variation with the velocity ν of the particle in suspension [8]:

$$\tau = \frac{A}{k\nu} \qquad (17)$$

where k is the wave number and A is a constant depending on the scattering properties of the sample.

Examining the results of the simulated time series we notice a decrease of the autocorrelation time with the ESR, although the correlation with Eq. (17) is not strong. This can be explained by the small number of SCs, which for this experiment was 500, as the computation time strongly increases with the SC number. The small number of SCs can be the cause for data points that are apart of the trend curve in Fig. 8.

CONCLUSION

The results of the computer simulation presented above were compared with the movies, with the time series and with the autocorrelation function recorded during a laboratory experiment performed on the real system that was simulated and were found to be realistic, therefore we can conclude that the computer simulation describes accurately both the far field interference aspect and the light scattering dynamics.

The computer simulation can be used further on to investigate the variation of the far field dynamics with the SC parameters like density, size, concentration, fluid viscosity, temperature and density.

The CHODIN code can be used to investigate the ESR variation with the RBC size and plasma parameters. The results of the simulation suggest a very fast experimental procedure for assessing the ESR, by processing the time series of coherent light scattered by RBCs in whole blood during sedimentation. The standard ESR analysis lasts for 40 minutes while recording a time series and calculating the autocorrelation function and ACT can be done in less than 2 minutes. Moreover, CHODIN can be used to simulate the effects of different drugs that modify the RBC size or physical plasma parameters on the autocorrelation time, or the presence of sickle anemia. These results of using CHODIN have to be proven by experimental work though.

The CHODIN computer code can be used to simulate the blood flow in both big and capillary vessels as well, by simply adjusting the input parameters. Work is in progress on this subject.

REFERENCES

1. AIZU, Y., T. ASAKURA, Bio-speckle phenomena and their application to the evaluation of blood flow, *Opt. Las. Tech.*, 1991, **23**, 205–219.
2. BERNE, B.J., R. PECORA, *Dynamic Light Scattering*, John Wiley, New York, 1976.

3.   BOAS, D.A., A.G. YODH, Spatially varying dynamical properties of turbid media probed with diffusing temporal light correlation, *J. Opt. Soc. Am. A.,* 1997, **14**, 192–215.
4.   BRIERS, J.D, G. RICHARDS, X.W. HE, Capillary blood flow monitoring using laser speckle contrast analysis (LASCA), *J. Biomed. Opt.,* 1999, **4**, 164–175.
5.   BRIERS, J.D., Laser Doppler, speckle and related techniques for blood perfusion mapping and imaging, *Physiol. Meas.*, 2001, **22**, R35–R66.
6.   DUBIN, S.B., J.H. LUNACEK, G.B. BENEDEK, Observation of the Spectrum of Light Scattered by Solutions of Biological Macromolecules, PNAS, 1967, **57**(5), 1164–1171.
7.   FEDOSOV, I.V., V.V. TUCHIN, The use of dynamic speckle field space time correlation function estimates for the direction and velocity determination of blood flow, *Proc. of SPIE,* 2001, **4434**, 192–196.
8.   GOODMAN, J.W., Statistical properties of laser speckle patterns, in *Laser Speckle and Related Phenomena*, Vol.9 in series *Topics in Applied Physics*, J.C. Dainty ed., Springer-Verlag, Berlin, Heidelberg, New York, Tokyo, 1984, pp. 9–77.
9.   GOODMAN, J.W., *Statistical Optics*, Wiley Classics Library Edition, New York, 2000.
10. HAMMER, M., D. SCHWEITZER, B. MICHEL, E. THAMM, A. KOLB, Single scattering by red blood cells, *Applied Optics,* 1998, **37**, 7410–7419.
11. HAMMER, M., A.N. YAROSLAVSKY, D. SCHWEITZER, A scattering phase function for blood with physiological haematocrit, *Physics in Medicine and Biology*, 2001, **46**, N65–N69.
12. HECHT, E., *Optics*, Addison-Wesley, New York, 2001.
13. KIM, I.C., S. TORQUATO, Effective conductivity of composites containing spheroidal inclusions: comparison of simulations with theory, *J. Appl. Phys.*, 1993, **74**(3), 1844–1854.
14. LUNACEK, N.A., J.H. CLARK, G.B. BENEDEK, A study of Brownian motion using light scattering, *American Journal of Physics*, 1970, **38**(5), 575–585.
15. ERTUGAY, M.F., M. SENGUL, M. SENGUL, Effect of ultrasound treatment on milk homogenisation and particle size distribution of fat, *Turk. J. Vet. Anim. Sci.*, 2004, **28**, 303–308.
16. PIEDERRIERE, Y., J. LE MEUR, J. CARIOU, J.F. ABGRALL, M.T. BLOUCH, Particle aggregation monitoring by speckle size measurement; application to blood platelets aggregation, *Optics Express*, 2004, **12**, 4596–4601.
17. PIEDERRIERE, Y, F. BOULVERT, J. CARIOU, B. LE JEUNE, Y. GUERN, G. LE BRUN, Backscattered speckle size as a function of polarization: influence of particle-size and concentration, *Optics Express* 2005, **13**, 5030–5039.
18. TSCHARNUTER, W., *Encyclopedia of Analytical Chemistry*, R.A. Meyers ed., John Wiley & Sons Ltd, 2000, 5469–5485.
19. WEINER, B.B., Chapter 5: Particle Sizing Using Ensemble Averaging Techniques, in *Liquid- and Surface-Borne Particle Measurement Handbook*, J.Z. Knapp, T.A. Barber, A. Liebermann eds., Marcel Dekker Inc., New York, 1996, pp. 55–172.
20. ZIMNYAKOV, D.A., J.D. BRIERS, V.V. TUCHIN, Chapter 18: Speckle technologies for monitoring and imaging of tissues and tissue like phantoms, in *Handbook of Biomedical Diagnostics*, Valery V. Tuchin ed., SPIE Press, Bellingham, 2002, pp. 2–48.